Ab Initio Treatment of the Chemical Reaction Precursor Complex Cl(^{2}P)−HF. 2. Bound States and Infrared Spectrum†

Anna V. Fishchuk, Gerrit C. Groenenboom, and Ad van der Avoird*

Institute of Theoretical Chemistry, IMM, Radboud University Nijmegen, Toernooiveld 1, 6525 ED Nijmegen, The Netherlands

Received: October 10, 2005; In Final Form: December 22, 2005

Bound energy levels and properties of the Cl(^{2}P)−HF complex were obtained from full three-dimensional (3D) calculations, with the use of the ab initio computed diabatic potential surfaces from the preceding paper and the inclusion of spin−orbit coupling. For a better understanding of the dynamics of this complex we also computed a 2D model in which the HF bond length r was frozen at the vibrationally averaged values r_0 and r_1 and a 2 + 1D model in which the 3D potentials were averaged over the $v_{HF} = 0$ and $v_{HF} = 1$ vibrational wave functions of free HF. Also 1D calculations were made in which both r and the Cl−HF distance R were frozen. The complex is found to have the linear hydrogen bonded Cl−HF structure, with ground-state quantum numbers $J = {}^3/_2$ for the overall angular momentum and $|\Omega| = {}^3/_2$ for its projection on the intermolecular axis **R**. The binding energy is $D_0 = 432.25$ cm^{-1} for $v_{HF} = 0$ and $D_0 = 497.21$ cm^{-1} for $v_{HF} = 1$. Bending modes with $|\Omega| = {}^1/_2$ and $|\Omega| = {}^5/_2$ are split by the Renner−Teller effect, since the electronic ground state is a degenerate $^2\Pi$ state. A series of intermolecular (R) stretch modes was identified. Rotational constants and e−f parity splittings were extracted from the levels computed for $J = {}^1/_2$ to ${}^7/_2$. The computed red shift of the HF stretch frequency of 64.96 cm^{-1} and the ^{35}Cl−^{37}Cl isotope shift of 0.033 cm^{-1} are in good agreement with the values of 68.77 and 0.035 cm^{-1} obtained from the recent experiment of Merritt et al. (*Phys. Chem. Chem. Phys.* **2005**, *7*, 67), after correction for the effect of the He nanodroplet matrix in which they were measured.

1. Introduction

The important role of van der Waals complexes occurring in the entrance and exit valleys of chemical reactions has been demonstrated on several examples.[1−6] The complex Cl(^{2}P)−HF that occurs in the entrance channel of the reaction Cl + HF → F + HCl was recently prepared in helium nanodroplets and studied by high-resolution infrared laser spectroscopy.[7] The preceding paper[8] describes the ab initio calculation and analytic representation of the full 3 × 3 matrix of diabatic potentials required to compute the bound states of this complex with the inclusion of the nonadiabatic Renner−Teller coupling. The diabatic electronic states of the complex correlate with the ^{2}P ground state of the Cl atom. In the present paper we use these potential surfaces, and include the spin−orbit coupling on the Cl(^{2}P) atom, to actually compute the Cl−HF bound states. All of the three internal degrees of freedom of Cl−HF were included in the calculations, but we also made one- and two-dimensional model calculations in order to elucidate the underlying dynamics. We discuss the bound state properties, and compare our theoretical results with the spectroscopic data, to verify that the potential surfaces from ref 8 are indeed accurate.

2. Bound State Calculations

The method to compute the bound states of open-shell atom−closed-shell diatom complexes of this type originates in work by Alexander[9] and by Dubernet and Hutson.[10,11] It is outlined in detail in ref 12. Reference 13 (see also the erratum[14]) gives results for the complex Cl(^{2}P)−HCl, which is similar to the Cl(^{2}P)−HF complex considered here. Still, as we show below, the properties of these two complexes are actually quite different. The theory in the previous papers[12,13] concerns two internal degrees of freedom; the HX bond length was frozen. Here, we perform full three-dimensional calculations with the Jacobi vectors **R**, the vector that points from the Cl nucleus to the center-of-mass of HF, and **r**, the vector that points from the H to the F nucleus, as dynamical variables. The internal coordinates varied are R, the length of **R**, r the HF bond length, and θ, the angle between **r** and **R**. The Hamiltonian in a body-fixed (BF) frame with its z-axis along **R** and **r** in the xz-plane is

$$\hat{H} = \hat{H}_{HF} + \frac{-\hbar^2}{2\mu_{AB}R}\frac{\partial^2}{\partial R^2}R + \frac{|\hat{\mathbf{j}}_A + \hat{\mathbf{j}}_B|^2 - 2(\hat{\mathbf{j}}_A + \hat{\mathbf{j}}_B)\cdot\hat{\mathbf{J}} + \hat{\mathbf{J}}^2}{2\mu_{AB}R^2} + A\hat{\boldsymbol{\lambda}}\cdot\hat{\mathbf{S}} + \sum_{\mu',\mu}|\lambda,\mu'\rangle\, V^{(\lambda)}_{\mu',\mu}(R, r, \theta)\,\langle\lambda,\mu| \quad (1)$$

where μ_{AB} is the reduced mass of the complex Cl−HF. The HF monomer Hamiltonian is

$$\hat{H}_{HF} = \frac{-\hbar^2}{2\mu_B r}\frac{\partial^2}{\partial r^2}r + \frac{\hat{\mathbf{j}}_B{}^2}{2\mu_B r^2} + V_{HF}(r) \quad (2)$$

and μ_B is the HF diatom reduced mass. The diatom potential $V_{HF}(r)$ was obtained from the spectroscopic data of Lonardo and Douglas[15] by the Rydberg−Klein−Rees (RKR) procedure.[16−19] The operators $\hat{\boldsymbol{\lambda}}$ and $\hat{\mathbf{S}}$ represent the orbital and spin angular momenta of the Cl(^{2}P) atom, respectively, and the atomic quantum numbers are $\lambda = 1$ and $S = {}^1/_2$. The operator $\hat{\mathbf{j}}_A = \hat{\boldsymbol{\lambda}} + \hat{\mathbf{S}}$ represents the total electronic angular momentum of the Cl atom, while $\hat{\mathbf{j}}_B$ is the rotational angular momentum of the diatom, and $\hat{\mathbf{J}}$ is the total angular momentum of the complex.

† Part of the special issue "John C. Light Festschrift".

* E-mail: A.vanderAvoird@theochem.ru.nl.

10.1021/jp0557621 CCC: $33.50
Published on Web 01/26/2006

The splitting between the spin−orbit states of the Cl atom is $D_{SO} = E(^2P_{1/2}) - E(^2P_{3/2}) = 882.4\ cm^{-1}$. We assume that the spin−orbit coupling in the open-shell Cl(^{2}P) atom is not affected by the relatively weak interaction with the HF molecule, so that we may use the atomic spin−orbit parameter $A = -(2/3)D_{SO}$ as a constant in eq 1. The 3 × 3 matrix of diabatic potentials $V^{(\lambda)}_{\mu,\mu'}(R,r,\theta)$ that couple the diabatic states $|\lambda,\mu\rangle$ with projection $\mu = -1, 0, 1$ on the z-axis was computed and described in ref 8. These interaction potentials are represented by the expansion

$$V^{(\lambda)}_{\mu',\mu}(R,r,\theta) = \sum_{l_B} C_{l_B,\mu-\mu'}(\theta,0)\ v^{(\lambda)\mu',\mu}_{l_B}(R,r) \qquad (3)$$

where $C_{l,m}(\theta,0)$ are Racah normalized spherical harmonics and the expansion coefficients $v^{(\lambda)\mu',\mu}_{l_B}(R,r)$ are given as functions of R and r by the reproducing kernel Hilbert space (RKHS) method;[20] see ref 8.

The basis to represent and diagonalize the Hamiltonian of eq 1 was the same as used for Cl−HCl in ref 13, except that we also need a basis for the coordinate $r \equiv r_{HF}$ now. This basis $|n_r\rangle \equiv \varphi_{n_r}(r)$ consists of contracted sinc−DVR functions,[21] with contraction coefficients chosen such that the functions $\varphi_{n_r}(r)$ are eigenfunctions with $j_B = 0$ of a reference Hamiltonian $\hat{H}_{HF} + V_{extra}(r)$. The additional potential $V_{extra}(r)$ is a scaled cut of the diabatic Cl−HF potential $V_{1,1}(R,r,\theta)$ with θ and R fixed at their equilibrium values $\theta_e = 0°$ and $R_e = 6.217\ a_0$. Its scaling factor of 0.7 was optimized by minimization of the ground-state energy of the Cl−HF complex in three-dimensional calculations. This is similar to the procedure used for the generation of the radial basis $|n_R\rangle \equiv \chi_{n_R}(R)$, where we used the isotropic component $v^{(\lambda)0,0}_0(R,r_e)$ of the diabatic Cl−HF potential $V_{0,0}(R,r_e,\theta)$ in the reference Hamiltonian. The HF bond length was fixed at the monomer equilibrium value $r_e = 1.7328\ a_0$. Here, because the radial Cl−HF potential is much shallower than the HF potential, we added a term $V_{extra}(R)$ linear in R in order to include the effect of continuum wave functions in the bound state basis. Also the slope of 175 cm^{-1}/a_0 of this linear term is optimized by minimization of the ground-state energy of the Cl−HF complex.

Because of the large spin−orbit coupling in the Cl(^{2}P) atom it is most convenient for the interpretation of the results to use a coupled atomic basis set

$$|j_A\omega_A\rangle \equiv |(\lambda S)\, j_A\omega_A\rangle = \sum_{\mu,\sigma} |\lambda,\mu\rangle|S,\sigma\rangle\langle\lambda,\mu;\, S,\, \sigma|j_A,\omega_A\rangle \quad (4)$$

for which the spin−orbit term $\hat{\lambda}\cdot\hat{\mathbf{S}} = (\hat{\mathbf{j}}_A^2 - \hat{\lambda}^2 - \hat{\mathbf{S}}^2)/2$ in the Hamiltonian is diagonal. The expression $\langle\lambda,\mu;S,\sigma|j_A,\omega_A\rangle$ is a Clebsch-Gordan coefficient. Since $\lambda = 1$ and $S = {}^1/_2$, one finds that $j_A = {}^1/_2$ and ${}^3/_2$.

The complete BF basis has the following form

$$|n_R,n_r,j_A,\omega_A,j_B,\omega_B,\Omega,J,M\rangle = \chi_{n_R}(R)\ \varphi_{n_r}(r)\left[\frac{2J+1}{4\pi}\right]^{1/2}|j_A,\omega_A\rangle\ Y_{j_B,\omega_B}(\theta,0)\ D^{(J)}_{M,\Omega}(\alpha,\beta,\phi)^* \quad (5)$$

where $Y_{jB,\omega B}(\theta,0)$ are spherical harmonics, and $D^{(J)}_{M,\Omega}(\alpha,\beta,\phi)^*$ are symmetric rotor functions. The Euler angles (α,β,ϕ) determine the orientation of the BF frame with respect to a space-fixed laboratory frame. The overall normalization factor differs from the normalization constant of $[(2J+1)/8\pi^2]^{1/2}$ of the symmetric rotor functions by a factor of $[2\pi]^{1/2}$. This factor is the normalization constant of the spherical harmonics $Y_{jB,\omega B}(\theta,0)$ with the azimuthal angle fixed at the value of zero. The components of angular momentum on the BF z-axis obey the relation $\Omega = \omega_A + \omega_B$. They are approximate quantum numbers. Exact quantum numbers are J, M, and the parity p of the states of the complex under inversion. A parity-adapted basis has the form

$$|n_R,n_r,j_A,\omega_A,j_B,\omega_B,\Omega,p,J,M\rangle = 2^{-1/2}[|n_R,n_r,j_A,\omega_A,j_B,\omega_B,\Omega,J,M\rangle + p(-1)^{\lambda-j_A+J}|n_R,n_r,j_A,-\omega_A,j_B,-\omega_B,-\Omega,J,M\rangle] \quad (6)$$

We remind the reader that ω_A and Ω adopt half-integer values only, so they cannot be equal to zero and the normalization factor of $1/\sqrt{2}$ in eq 6 holds for all basis functions. In the sequel we use the spectroscopic parity defined by $\epsilon = p(-1)^{J-S}$. States with $\epsilon = 1$ and $\epsilon = -1$ are labeled e and f, respectively.

In addition to the full 3D-calculations we also made one-dimensional (1D) and two-dimensional (2D and 2 + 1D) calculations. The 1D calculations were performed by fixing r at $r_e = 1.7328\ a_0 = 0.9170$ Å and fixing R for a series of R values ranging from 2.5 to 5.0 Å. For the HF rotational constant we chose $B_{v=0} = 20.5598\ cm^{-1}$. These calculations were mainly intended to better understand the hindered internal rotation of the HF monomer and the coupling of the diabatic electronic states.

The 2D calculations were made with the basis $|n_R\rangle|j_A,\omega_A,j_B,\omega_B,\Omega,J,M\rangle$, while the r coordinate was frozen either at the HF equilibrium value $r_e = 0.9170$ Å, or at one of the vibrationally averaged values, $\langle r\rangle_0 = 0.9326$ Å or $\langle r\rangle_1 = 0.9649$ Å, depending on the HF vibrational state $v_{HF} = 0$ or $v_{HF} = 1$ that we wish to consider. In the 2D calculations with $r = r_e$ and $r = r_0$, we used the HF rotational constant $B_0 = 20.5598\ cm^{-1}$, while $B_1 = 19.7855\ cm^{-1}$ was taken in the 2D calculation with $r = r_1$. In the treatment called 2 + 1D we averaged the full 3D diabatic potentials over the vibrational wave functions of HF with $v_{HF} = 0$ and $v_{HF} = 1$. This is equivalent to the use of the full 3D basis with n_r restricted to the values $n_r = 0$ or $n_r = 1$, with the condition that the basis functions $|n_r\rangle$ are eigenfunctions of the bare HF Hamiltonian $\hat{H}_{HF}$. That is, the potential $V_{extra}(r)$ added in the generation of the contracted sinc−DVR basis $|n_r\rangle$ must be omitted here. The 1D calculations were made with the basis $|j_A,\omega_A,j_B,\omega_B,\Omega,J,M\rangle$.

The 3D bound states were obtained from a full diagonalization of the Hamiltonian matrix for $J = {}^1/_2$ and ${}^3/_2$. The basis $|n_R\rangle$ is included with $n_R^{max} = 13$, the basis $|n_R\rangle$ is included with $n_r^{max} = 6$, and the quantum number j_B in the angular basis has a maximum value of 13. Convergence tests have shown that the increase of n_R^{max} from 13 to 14 gives a lowering of the relevant energy levels smaller than $10^{-3}\ cm^{-1}$, the increase of n_r^{max} from 6 to 7 a lowering of less than $10^{-5}\ cm^{-1}$, and the increase of j_B^{max} from 13 to 14 also a lowering of less than $10^{-5}\ cm^{-1}$. The same value $j_B^{max} = 13$ was used in the 1D, 2D, and 2 + 1D calculations and the R basis in the 2D and 2 + 1D calculations was truncated at $n_R^{max} = 13$ as well. Full 3D calculations for J values higher than ${}^3/_2$ were not performed because they are quite expensive, but the 2D and 2 + 1D calculations were carried out for J values up to ${}^7/_2$.

3. Results and Discussion

3.1. Diabatic and Adiabatic Potentials Including Spin−Orbit Coupling. For a better understanding of the bound states of the Cl(^{2}P)−HF complex, it is useful to consider diabatic and adiabatic energy surfaces including the large spin−orbit coupling. Diabatic states $|j_A\omega_A\rangle$ including spin−orbit coupling are defined which correlate to the atomic states $|j_A\omega_A\rangle \equiv |(\lambda S)$-$j_A\omega_A\rangle$ of eq 4. The corresponding diabatic potentials $V_{j'_A,\omega'_A;j_A,\omega_A}$-

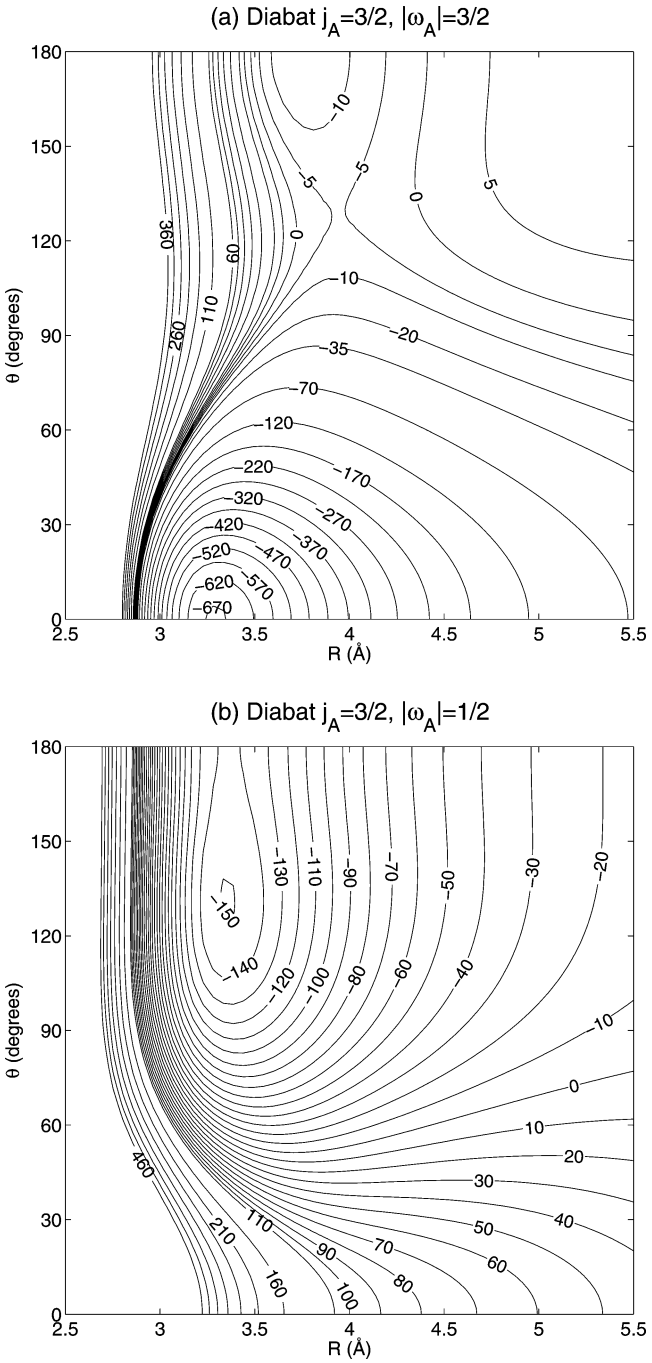

Figure 1. Diabatic potential energy surfaces for Cl(^{2}P)−HCl including spin−orbit coupling for $j_A = {}^3/_2$. Energy (in cm^{-1}) relative to the ground Cl ($^2P_{3/2}$) state.

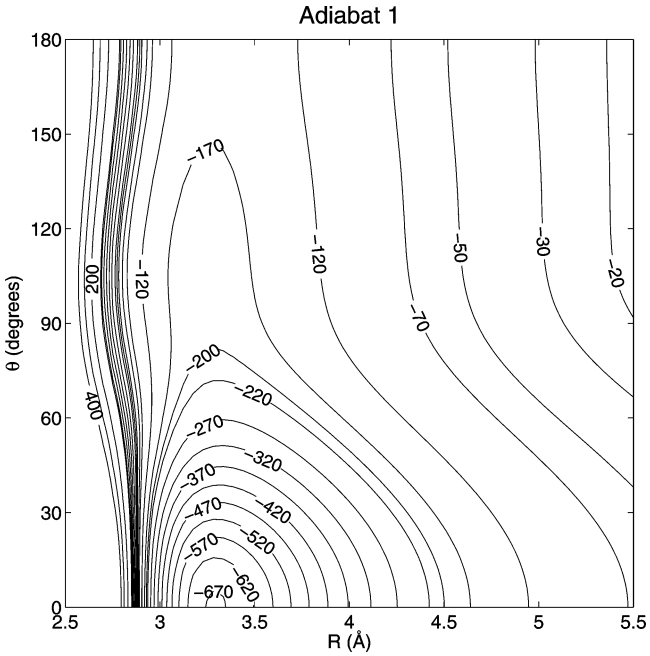

Figure 2. Lowest adiabatic potential energy surface for Cl(^{2}P)−HCl including spin−orbit coupling. Energy (in cm^{-1}) relative to the ground Cl ($^2P_{3/2}$) state.

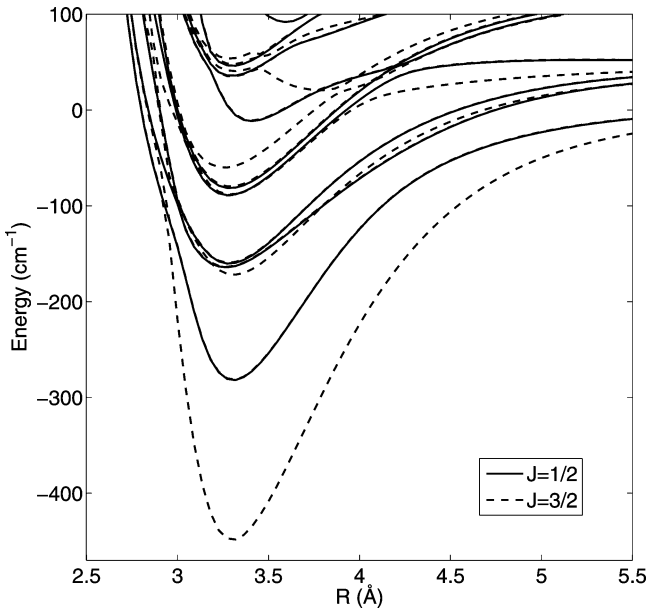

Figure 3. Bound levels from 1D calculations with fixed R and $r = r_e$, as functions of R. Closed lines correspond to $J = {}^1/_2$ and dashed lines to $J = {}^3/_2$.

$(R,r,\theta) \equiv \langle j'_A \omega'_A | \hat{V} + \hat{H}_{SO} | j_A \omega_A \rangle$ are the matrix elements of the operator

$$\hat{V} + \hat{H}_{SO} = \sum_{\mu',\mu} |\lambda,\mu'\rangle \, V^{(\lambda)}_{\mu',\mu}(R,r,\theta) \, \langle \lambda,\mu| + A\hat{\lambda}\cdot\hat{S} \qquad (7)$$

The spin−orbit term is constant and diagonal in this basis. The two diagonal potentials $V_{j_A,\omega_A;j_A,\omega_A}$ with $j_A = {}^3/_2$ that correlate with the $^2P_{3/2}$ ground state of the Cl atom are plotted in Figure 1, parts a and b. The diabatic potential for $|\omega_A| = {}^3/_2$ is similar to the diabat $V_{1,1}$, see Figure 6 of ref 8, and it has the same minima for the linear structures with $\theta = 0°$ and $\theta = 180°$. The diabat for $|\omega_A| = {}^1/_2$ qualitatively resembles the $V_{0,0}$ diabat in Figure 5 of ref 8, but has an even shallower minimum near $\theta = 130°$. Adiabatic potentials are obtained by diagonalization of the 6 × 6 matrix with the spin−orbit coupling included diabats, or alternatively, by the diagonalization of a complex valued 3 × 3 matrix.[22] The lowest adiabatic potential including spin−orbit coupling plotted in Figure 2 is not very different from the lowest adiabat $V_1(A')$ without spin−orbit coupling, see Figure 2 of ref 8, but the local minimum for a nonlinear geometry is almost absent now. This situation is very different from the Cl−HCl case,[13,14] where the $|\omega_A| = {}^1/_2$ diabat has a pronounced minimum at the T-shaped geometry and the lowest adiabat with spin−orbit coupling included has two minima of nearly equal depth at $\theta = 0°$ and $\theta \approx 90°$. We will show below that this has important consequences for the characteristics of these complexes.

3.2. 1D Calculations. The 1D calculations were made for R values ranging from 2.5 to 5.5 Å in steps of 0.05 Å with r fixed

TABLE 1: Results from Different Models: Binding Energies D_0 (parity e, $J = {}^3/_2$) and D_e and Equilibrium Distances R_e

	$v_{HF} = 0$			$v_{HF} = 1$		
model	D_0 (cm^{-1})	D_e (cm^{-1})	R_e (Å)	D_0 (cm^{-1})	D_e (cm^{-1})	R_e (Å)
2D ($r = r_e$)	405.44	676.50	3.2897			
2D ($r = r_v$)	421.20	699.65	3.2866	461.06	751.95	3.2782
2 + 1D	429.55	713.59	3.2795	493.10	801.70	3.2568
3D	432.25	678.50[a]	3.2891	497.21		

[a] Relative to D_e of free HF; r_e has increased from 0.9170 to 0.9199 Å, and the intermolecular contribution is 680.77 cm^{-1}.

at the HF equilibrium bond length $r_e = 0.9170$ Å. They result in the energies curves plotted in Figure 3 for $J = {}^1/_2$ and ${}^3/_2$. The lowest curve corresponds to $J = {}^3/_2$. The second lowest curve has $J = {}^1/_2$, and nearly coincides with the second $J = {}^3/_2$ curve. This already indicates that $|\Omega|$ is a nearly good quantum number, with the lowest curve corresponding to $|\Omega| = {}^3/_2$ and the next two curves to $|\Omega| = {}^1/_2$. The very small energy difference between the $|\Omega| = {}^1/_2$ curves for $J = {}^1/_2$ and $J = {}^3/_2$ is from the end-over-end rotation of the complex. In contrast with the Cl−HCl case[13,14] all minima occur for approximately the same value of $R \approx 3.3$ Å. This value of R is close to the R_e value of the linear Cl−HF minimum in the lowest diabat with $j_A = |\omega_A| = {}^3/_2$, which is also the minimum in the lowest adiabat. We will see below that this indicates that all the lower bound states are localized near a single linear equilibrium geometry of Cl−HF.

3.3. 2D Calculations. Let us first discuss how well the models 2D and 2 + 1D agree with the full 3D results. An overview of the D_0 values from different models is given in Table 1, together with the relevant D_e and R_e values. We observe in the 2D results with r_0 and r_1, and from the comparison of these results with those of 2D calculations at $r = r_e$, that a change of the (fixed) value of r has a large effect on both D_e and D_0. This is not surprising, given the strong increase of the well depth D_e in the 3D potential when r is increased; see Table 2 of ref 8. There is also a substantial difference between the results from the models 2D and 2 + 1D. It is clear from Table 1 that model 2 + 1D gives results that are much closer to the full 3D results than model 2D. Actually, the difference between model 2 + 1D and the 3D calculations is considerably smaller than the difference among the models 2 + 1D and 2D. A similar conclusion was reached by Jeziorska et al.[23] in a study on the more weakly bound closed-shell Ar−HF complex, but the deviations between the different models 2D and 2 + 1D and the 3D model are much more pronounced for Cl−HF.

Table 2 lists the rovibronic levels for $J = {}^1/_2$, ${}^3/_2$, ${}^5/_2$, and ${}^7/_2$, from model 2 + 1D, with the 3D potentials averaged over the $v = 0$ wave functions of HF. Table 3 contains the parity splittings between the levels of e and f symmetry. As $|\Omega|$ is a

TABLE 2: Lowest Bound States of e Parity, from the 2 + 1D Model with $v_{HF} = 0$[a]

$\|\omega_A\|$	$\|\omega_B\|$	v_b	v_s	$J = {}^1/_2$	$J = {}^3/_2$	$J = {}^5/_2$	$J = {}^7/_2$
				$\|\Omega\| = {}^1/_2$			
${}^3/_2$	1	1	0	−261.2337 (−263.0226)	−260.9376 (−262.7259)	−260.4049	−259.6355
${}^3/_2$	1	1	1	−193.9466 (−195.3645)	−193.6699 (−195.0871)	−193.1682	−192.4415
${}^1/_2$	0			−146.0861 (−146.5588)	−145.8456 (−146.3161)	−145.3637	−144.6392
${}^1/_2$	1		0	−140.4824 (−141.2333)	−140.1671 (−140.9175)	−139.6034	−138.7914
			2	−134.6425 (−135.6009)	−134.4187 (−135.3801)	−133.9762	−133.3156
${}^1/_2$	0			−102.4815 (−102.8389)	−102.3325 (−102.6983)	−101.9737	−101.4022
${}^1/_2$	1		1	−90.3787 (−90.9079)	−90.0246 (−90.5513)	−89.4388	−88.6213
			3	−87.1604 (−87.8795)	−86.9726 (−87.6937)	−86.5798	−85.9828
${}^1/_2$	1		0	−70.0935 (−70.9383)	−69.5540 (−70.3971)	−68.7850	−67.7878
${}^1/_2$	0			−65.6496 (−65.9835)	−65.4943 (−65.8312)	−65.1290	−64.5523
${}^1/_2$	0			−62.1719 (−63.0668)	−62.1463 (−63.0393)	−61.8657	−61.3282
				−50.2016 (−50.7026)	−49.9841 (−50.4858)	−49.5866	−49.0086
${}^1/_2$	1		2	−46.3278 (−46.7253)	−46.0665 (−46.4621)	−45.5836	−44.8792
					$\|\Omega\| = {}^3/_2$		
${}^3/_2$	0	0	0		−429.5538 (−432.2490)	−428.9598	−428.1283
${}^3/_2$	0	0	1		−348.2344 (−350.5154)	−347.6666	−346.8716
${}^3/_2$	0	0	2		−276.2444 (−278.1656)	−275.7030	−274.9451
${}^3/_2$	0	0	3		−213.1933 (−214.7899)	−212.6801	−211.9617
${}^3/_2$	0	0	4		−159.3109 (−160.6016)	−158.8231	−158.1405
					−151.3275 (−152.4041)	−150.7683	−149.9869
${}^3/_2$	0	0	5		−113.6856 (−114.7123)	−113.2327	−112.5990
					−100.6460 (−101.3913)	−100.0702	−99.2949
${}^3/_2$	0	0	6		−75.8692 (−76.6765)	−75.4514	−74.8672
${}^1/_2$	1				−71.5921 (−72.5423)	−71.0805	−70.3682
					−55.3705 (−55.9905)	−54.8277	−54.0774
${}^3/_2$	0	0	7		−42.8889 (−43.6463)	−42.4824	−41.9132
${}^1/_2$	2		0		−40.2745 (−40.8528)	−39.6167	−38.7076
					$\|\Omega\| = {}^5/_2$		
${}^3/_2$	1	1	0			−221.7005	−220.8855
${}^3/_2$	1	1	1			−155.7650	−154.9945
${}^3/_2$	1	1	2			−99.9218	−99.1501
${}^3/_2$	1	1	3			−55.2584	−54.5886
						−45.7152	−44.9850
${}^3/_2$	1	1	4			−18.2666	−17.6568
						−2.3564	−1.6270
					$\|\Omega\| = {}^7/_2$		
${}^3/_2$	2		0				−38.2758

[a] Energies in cm^{-1} relative to the energy of Cl(^{2}P$_{3/2}$) and HF($v = 0$). The numbers in parentheses are from 3D calculations. Quantum numbers v_s and v_b refer to the intermolecular stretch and bend.

TABLE 3: Parity Splittings $\Delta E = E_f - E_e$ in cm^{-1}, for $v_{HF} = 0$

$\lvert\omega_A\rvert$	$\lvert\omega_B\rvert$	v_b	v_s	$J = 1/2$	$J = 3/2$	$J = 5/2$	$J = 7/2$
				$\lvert\Omega\rvert = 1/2$			
3/2	1	1	0	0.1182 (0.1174)	0.2363 (0.2349)	0.3544	0.4723
3/2	1	1	1	0.1217 (0.1208)	0.2433 (0.2414)	0.3648	0.4860
1/2	0			0.2372 (0.2292	0.4714 (0.4558)	0.7000	0.9202
1/2	1		0	0.1150 (0.1122)	0.2291 (0.2233)	0.3413	0.4505
			2	0.2115 (0.2211)	0.4246 (0.4443)	0.6413	0.8635
1/2	0			0.3108 (0.3093)	0.6077 (0.5905)	0.8812	1.1282
1/2	1		1	−0.0150 (−0.0214)	−0.0316 (−0.0445)	−0.0515	−0.0765
			3	0.2428 (0.2497)	0.4876 (0.5016)	0.7366	0.9921
1/2	1		0	−0.3863 (−0.3882)	−0.7706 (−0.7746)	−1.1510	−1.5250
1/2	0			0.3126 (0.3172)	0.6216 (0.6305)	0.9237	1.2159
1/2	0			0.7050 (0.7033)	1.4052 (1.4024)	2.0954	2.7698
				0.1056 (0.1085)	0.2123 (0.2180)	0.3210	0.4323
1/2	1		2	0.1411 (0.1364)	0.2810 (0.2717)	0.4184	0.5523
				$\lvert\Omega\rvert = 3/2$			
3/2	0	0	0		0.0000 (0.0000)	0.0000	0.0000
3/2	0	0	1		0.0000 (0.0000)	0.0000	0.0000
3/2	0	0	2		0.0000 (0.0000)	0.0000	0.0000
3/2	0	0	3		0.0000 (0.0000)	0.0000	0.0000
3/2	0	0	4		0.0000 (0.0000)	0.0001	0.0003
					0.0018 (0.0016)	0.0073	0.0180
3/2	0	0	5		0.0000 (0.0000)	0.0001	0.0004
					0.0131 (0.0274)	0.0423	0.2069
3/2	0	0	6		0.0001 (0.0001)	0.0003	0.0006
1/2	1				0.0045 (0.0045)	0.0175	0.0429
					0.0011 (0.0010)	0.0044	0.0113
3/2	0	0	7		0.0001 (0.0001)	0.0004	0.0012
1/2	2		0		0.0005 (0.0005)	0.0020	0.0047

nearly good quantum number the energy levels in Table 2 are sorted according to their $|\Omega|$ values. Values in the same row for increasing $J \geq |\Omega|$ clearly correspond to end-over-end rotational progressions of the same internal state. The approximate quantum numbers $|\omega_A|$ and $|\omega_B|$ were obtained from an analysis of the wave functions. They are assigned only when the value indicated for each quantum number has a probability of at least 60%. The bending and intermolecular (R) stretch quantum numbers v_b and v_s of the complex were determined from contour plots of the density distributions as shown in Figure 4 and are based on counting the nodes in these plots.

In Table 2, one can see that the ground state of the complex with energy $E = -429.55$ cm^{-1} has $J = 3/2$ and $|\Omega| = 3/2$ and is dominated by the diabatic state with $j_A = |\omega_A| = 3/2$. The bend mode is not excited and $\omega_B = 0$. In Figure 4a, one observes that this ground state is localized near the global minimum in the $j_A = |\omega_A| = 3/2$ diabat at the linear Cl−HF structure; see Figure 1a. In similar plots, we could verify that the series of higher levels in Table 2 with the same electronic and angular quantum numbers as the ground state and increasing values of v_s correspond to a clear intermolecular stretch progression up to $v_s = 7$ inclusive. Figure 4b is the plot for $v_s = 1$; plots of the levels with higher v_s are not shown. Figure 4c shows one of the higher states for which no approximate quantum numbers other than $|\Omega| = 3/2$ could be assigned. It is delocalized over a wide range of the bending angle θ.

In contrast with the Cl−HCl complex,[13,14] where the lowest levels with $|\Omega| = 1/2$ correspond to a T-shaped "isomer", the levels for $|\Omega| = 1/2$ in Cl−HF are clearly bend fundamental $v_b = 1$ excited levels of a linear complex; see Figure 4d. The quantum number $|\omega_B| = 1$ represents the vibrational angular momentum of this bend mode. Also Figure 3 confirms this picture; the lowest curve with $J = |\Omega| = 1/2$ has nearly the same radial minimum as the ground state, whereas for Cl−HCl,[13,14] the corresponding curve has a minimum at a much smaller value of R, indicative of a T-shaped structure. Figure 4e shows the first bend−stretch combination state of Cl−HF with $v_b = 1$ and $v_s = 1$. The next state with $|\Omega| = 1/2$, shown in Figure 4f is delocalized and does not have any well-defined bend or stretch quantum numbers.

The parity splitting $E_f - E_e$ of the $|\Omega| = 1/2$ levels in Table 3 increases linearly with $J + 1/2$, as is customary in linear open-shell triatomic molecules.[24] In our calculations, it originates from off-diagonal Coriolis coupling terms in the Hamiltonian of eq 1 containing the shift operators J_+ and J_- that couple basis functions with $\Omega = \pm 1/2$. Also the fact that the splitting is smaller by several orders of magnitude for the $|\Omega| = 3/2$ levels is commonly observed in such systems. It can be understood from the fact that functions with $\Omega = \pm 3/2$ can only be coupled indirectly.

The levels obtained from the 2 + 1D model with the 3D potentials averaged over the $v = 1$ wave functions of HF are shown in Table 4, and the corresponding parity splittings are shown in Table 5. The different characteristics of the Cl−HF complex in the $v = 0$ and $v = 1$ states of the HF stretch vibration will be discussed in the next section.

3.4. 3D Calculations and Spectroscopic Properties. The numbers given in parentheses in Tables 2 and 3 are from full 3D calculations. One observes that the levels and splittings from the 2 + 1D model agree quite well with the 3D results: not only the D_0 values but also the excited bound levels. The same observation holds for the calculated levels of Cl−HF with the HF stretch vibration excited; see Tables 4 and 5. It was not hard to recognize the levels that correspond to $v_{HF} = 1$ in the 3D calculations, because the $v_{HF} = 1$ character is conserved to a large extent in the Cl−HF complex. Also, the expectation value of r over the 3D wave functions has not increased much with respect to free HF: it is 0.9358 and 0.9693 Å in the $v_{HF} = 0$ and $v_{HF} = 1$ states, respectively, while the corresponding values for free HF are 0.9326 and 0.9649 Å. Hence, the reaction

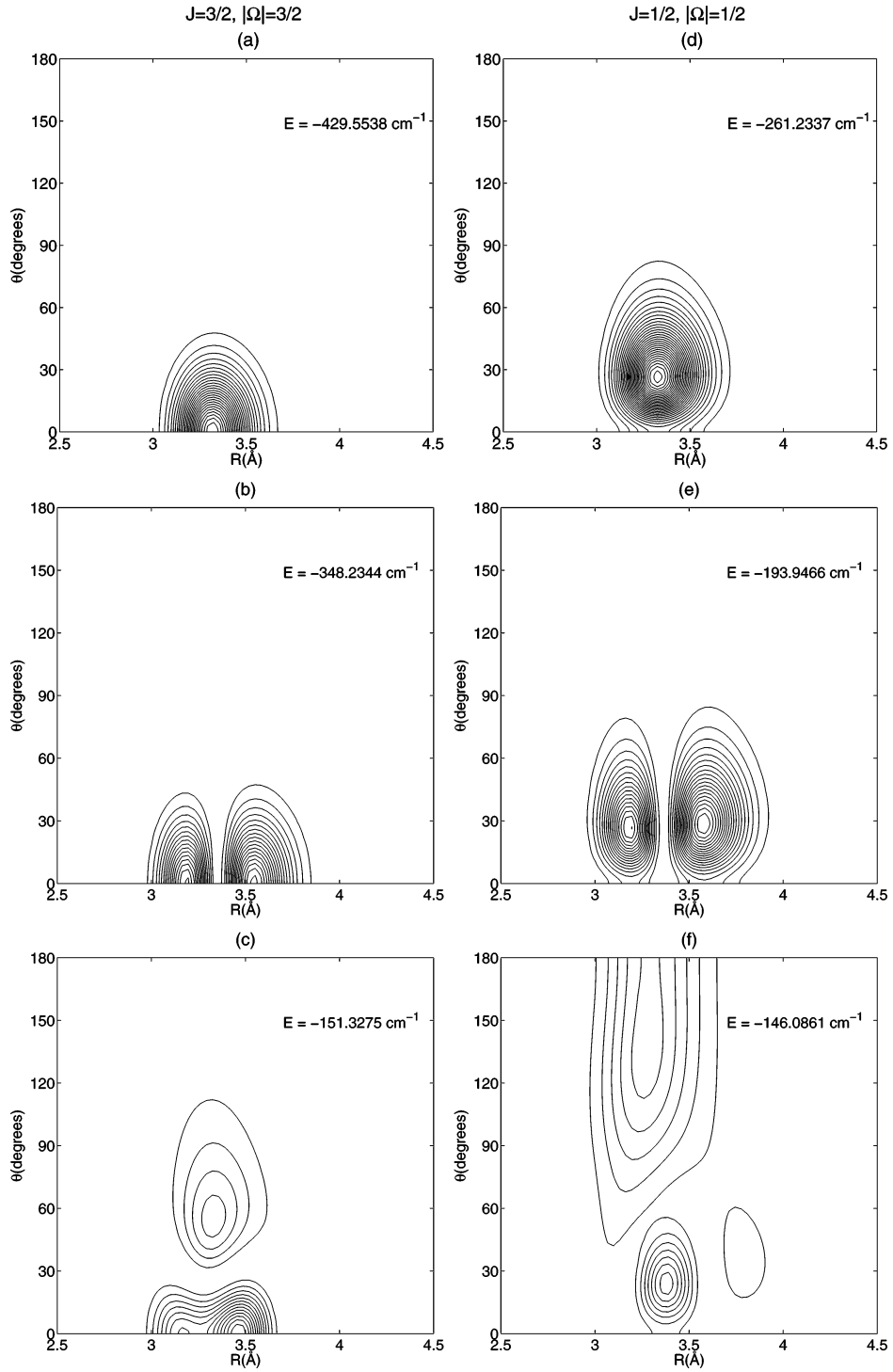

Figure 4. Density distributions from the 2 + 1D model for $v_{HF} = 0$. They are obtained by integration of the absolute squared wave functions over the electronic coordinates and overall rotation angles (α,β,ϕ) of the complex. The corresponding energies and quantum numbers are given in Table 2.

Cl + HF → HCl + F has not started yet. This is probably a consequence of the fact that this reaction is endothermic and has a high activation energy barrier.

Starting from the ground level with $J = {}^3/_2$ and $|\Omega| = {}^3/_2$ we could identify an intermolecular stretch progression with quantum numbers up to $v_s = 7$. A fit of this progression to the usual formula with anharmonic corrections

$$E(v_s) = E_e + \omega_e\left(v_s + \frac{1}{2}\right) - \omega_e x_e\left(v_s + \frac{1}{2}\right)^2 + \omega_e y_e\left(v_s + \frac{1}{2}\right)^3 \quad (8)$$

after first removing the parity splittings by averaging the energies over the states of parities e and f yields the spectroscopic parameters listed in Table 6. We saw already in Table 1 that D_0 is considerably increased when the HF stretch is excited, $v_{HF} = 0 \rightarrow 1$. We see now that also the intermolecular stretch frequency increases, from 91.0 to 97.1 cm^{-1}. Similar, but shorter, stretch progressions are found for the bend excited levels with $|\Omega| = {}^1/_2$ and $|\Omega| = {}^5/_2$. The bend mode itself will be addressed in section 3.5, where we discuss the Renner−Teller effects.

TABLE 4: Lowest Bound States of e Parity, from the 2 + 1D Model with $v_{HF} = 1$[a]

$\|\omega_A\|$	$\|\omega_B\|$	v_b	v_s	$J = 1/2$	$J = 3/2$	$J = 5/2$	$J = 7/2$
				$\|\Omega\| = 1/2$			
3/2	1	1	0	−305.8188 (−308.5402)	−305.5139 (−308.3727)	−304.9686	−304.1831
3/2	1	1	1	−232.4841 (−234.7224)	−232.1962 (−234.4997)	−231.6791	−230.9329
3/2	1	1	2	−170.4741 (−172.0316)	−170.2090 (−171.8991)	−169.7228	−169.0156
1/2			0	−165.5586 (−166.8322)	−165.1738 (−166.4457)	−164.5458	−163.6746
1/2	0			−154.0743 (−154.6339)	−153.9330 (−154.5768)	−153.5441	−152.9078
			3	−119.4185 (−120.4937)	−119.1892 (−120.2641)	−118.7414	−118.0739
1/2			1	−110.2662 (−111.1106)	−109.8728 (−110.7170)	−109.2488	−108.3946
1/2	0			−106.3365 (−106.9718)	−106.2070 (−106.8453)	−105.8475	−105.2580
1/2	1		0	−91.0916 (−92.1430)	−90.5518 (−91.6021)	−89.7726	−88.7543
1/2	0		0	−81.8935 (−82.9889)	−81.8508 (−82.9468)	−81.5426	−80.9668
1/2	0			−78.9523 (−79.6258)	−78.7759 (−79.4489)	−78.3993	−77.8227
1/2				−66.2106 (−66.8504)	−65.9903 (−66.5896)	−65.5909	−65.0174
1/2	1		2	−61.6129 (−62.2231)	−61.3668 (−61.9793)	−60.8961	−60.2010
					$\|\Omega\| = 3/2$		
3/2	0	0	0		−493.1007 (−497.2113)	−492.4973	−491.6529
3/2	0	0	1		−405.5453 (−409.0480)	−404.9666	−404.1565
3/2	0	0	2		−327.5110 (−330.4497)	−326.9571	−326.1817
3/2	0	0	3		−258.3686 (−260.8759)	−257.8409	−257.1024
3/2	0	0	4		−198.0680 (−200.1500)	−197.5686	−196.8697
			0		−176.5718 (−178.2383)	−175.9863	−175.1670
3/2	0	0	5		−146.2354 (−147.9346)	−145.7679	−145.1137
			1		−121.0808 (−122.2300)	−120.5353	−119.7743
3/2	0	0	6		−102.4315 (−103.7320)	−101.9986	−101.3927
1/2	1				−91.4749 (−92.5790)	−90.9556	−90.2317
					−72.5949 (−73.5255)	−72.0923	−71.3903
3/2	0	0	7		−65.8273 (−66.8902)	−65.3668	−64.7105
1/2	2		0		−58.6923 (−59.3994)	−58.0356	−57.1183
					$\|\Omega\| = 5/2$		
3/2	1	1	0			−264.5033	−263.6748
3/2	1	1	1			−192.9310	−192.1439
3/2	1	1	2			−131.5474	−130.8035
3/2	1	1	3			−80.7108	−80.0022
1/2	2					−66.7180	−65.4614
3/2	1	1	4			−38.7966	−38.1467
						−20.5068	−19.7705
				$\|\Omega\| = 7/2$			
3/2	2		0				−66.7107

[a] Energies are given in cm^{-1} relative to the energy of $Cl(^2P_{3/2})$ and HF ($v = 1$). The numbers in parentheses are from 3D calculations.

From the series of levels computed for $J = 1/2$ to $7/2$ with the 2 + 1D model one can extract a rotational constant B and a distortion constant D by a fit to the linear molecule expression

$$E(J) = E_0 + B[J(J+1) - \Omega^2] - D[J(J+1) - \Omega^2]^2 \quad (9)$$

Again, we first removed the parity splittings by averaging the energies over the states of parities e and *f*. The values are included in Table 6. The rotational constant B increases from 0.1188 to 0.1207 cm^{-1} when the HF stretch is excited, in agreement with the finding that the complex is more strongly bound and has a smaller R_e value for $v_{HF} = 1$ than for $v_{HF} = 0$.

The amount by which the HF stretch frequency in the Cl−HF complex is red-shifted from the free HF value of 3961.2 cm^{-1} is shown in Table 7. The results refer to the levels of e parity, but the results for f parity are practically the same. The value from the 2D model is substantially lower than the full 3D value of 64.96 cm^{-1}, but the 2 + 1D model underestimates the 3D value by only 1.41 cm^{-1}. Apparently, the origin of the red shift is not so much the dynamical coupling between the HF stretch mode and the intermolecular modes, but rather the fact that the Cl−HF binding energy D_0 is much larger for $v_{HF} = 1$ than for $v_{HF} = 0$. This red shift was measured by Merritt et al.[7] for Cl−HF prepared in cold He nanoclusters. The experimental value is 73.69 cm^{-1}. We may correct this value for the He matrix effect by using the red shifts of HF−HF, which were observed both in the gas phase and in He clusters.[25] The red shift of the stretch frequency of the donor HF molecule in the dimer is 93.26 cm^{-1} in the gas phase and 99.39 cm^{-1} in He clusters, the corresponding shifts of the acceptor HF molecule are 30.45 and 33.48 cm^{-1}. Linear interpolation of the frequency shift $\Delta\nu$ between these values with the formula

$$\Delta\nu^{gas}_{Cl-HF} = \Delta\nu^{gas}_{HF-HF\ acceptor} + (\Delta\nu^{cluster}_{Cl-HF} - \Delta\nu^{cluster}_{HF-HF\ acceptor}) \times \frac{\Delta\nu^{gas}_{HF-HFdonor} - \Delta\nu^{gas}_{HF-HF\ acceptor}}{\Delta\nu^{cluster}_{HF-HFdonor} - \Delta\nu^{cluster}_{HF-HF\ acceptor}} \quad (10)$$

and the Cl−HF red shift of 73.69 cm^{-1} measured in He gives an estimate of the matrix shift $\Delta\nu^{cluster} - \Delta\nu^{gas}$ for Cl−HF of 4.92 cm^{-1}. Use of the values measured for the HCN−HCN dimer[26] would produce a similar matrix shift. With the inclusion of this estimated matrix effect the experimental red shift in gas-phase Cl−HF is 68.77 cm^{-1}, in quite good agreement with our best 3D calculated value of 64.96 cm^{-1}.

Actually, all lines in the experimental spectrum are doublets, caused by the fact that for Cl two isotopes, ^{35}Cl and ^{37}Cl, exist in natural abundances of about 3 to 1. All the lines assigned to ^{37}Cl−HF are lower in frequency by 0.038 cm^{-1} than the lines due to ^{35}Cl−HF. With a similar correction for the He matrix effect as applied to the red shift, we estimate the isotope shift in the gas phase to be 0.035 cm^{-1}. Harmonic ab initio calculations[7] completely failed to reproduce this isotope effect; they gave a shift smaller than 10^{-4} cm^{-1}. We performed all

TABLE 5: Parity Splittings $\Delta E = E_f - E_e$ in cm^{-1}, for $v_{HF} = 1$

$\lvert\omega_A\rvert$	$\lvert\omega_B\rvert$	v_b	v_s	$J = {}^1/_2$	$J = {}^3/_2$	$J = {}^5/_2$	$J = {}^7/_2$
				$\lvert\Omega\rvert = {}^1/_2$			
$^3/_2$	1	1	0	0.1113 (0.1253)	0.2225 (0.3771)	0.3336	0.4447
$^3/_2$	1	1	1	0.1120 (0.1072)	0.2241 (0.2993)	0.3360	0.4478
$^3/_2$	1	1	2	0.1332 (−0.0367)	0.2662 (0.2717)	0.3988	0.5306
$^1/_2$			0	−0.0403 (−0.0404)	−0.0809 (−0.0832)	−0.1219	−0.1637
$^1/_2$	0			0.4602 (0.4651)	0.9202 (1.0069)	1.3802	1.8401
			3	0.1920 (0.1826)	0.3816 (0.3789)	0.5665	0.7442
$^1/_2$			1	−0.0949 (−0.0939)	−0.1898 (−0.1878)	−0.2849	−0.3801
$^1/_2$	0			0.4318 (0.4355)	0.8638 (0.8752)	1.2962	1.7289
$^1/_2$	1		0	−0.3579 (−0.3589)	−0.7100 (−0.7137)	−1.0430	−1.5136
$^1/_2$	0		0	0.6995 (0.7015)	1.3910 (1.3955)	2.0652	2.7098
$^1/_2$	0			0.2487 (0.2425)	0.4989 (0.4875)	0.7531	1.0183
$^1/_2$				0.0991 (0.1041)	0.2485 (0.1969)	0.3982	0.5725
$^1/_2$	1		2	0.1791 (0.1836)	0.3568 (0.4048)	0.5321	0.7045
				$\lvert\Omega\rvert = {}^3/_2$			
$^3/_2$	0	0	0		0.0000 (0.0000)	0.0000	0.0000
$^3/_2$	0	0	1		0.0000 (0.0001)	0.0000	0.0000
$^3/_2$	0	0	2		0.0000 (0.0535)	0.0000	0.0000
$^3/_2$	0	0	3		0.0000 (0.0200)	0.0000	0.0000
$^3/_2$	0	0	4		0.0000 (0.0000)	0.0000	0.0000
			0		0.0003 (0.0270)	0.0013	0.0032
$^3/_2$	0	0	5		0.0000 (0.0012)	0.0002	0.0000
			1		0.0020 (0.0010)	0.0080	0.0201
$^3/_2$	0	0	6		0.0001 (0.0001)	0.0003	0.0009
$^1/_2$	1				−0.0004 (0.0011)	−0.0098	0.1333
					0.0008 (0.0394)	0.0032	0.0080
$^3/_2$	0	0	7		−0.0499 (0.0086)	−0.0991	−0.1718
$^1/_2$	2		0		0.0011 (0.0013)	0.0040	0.0093

TABLE 6: Spectroscopic Parameters in cm^{-1}

	2+1D model		3D model	
	$v_{HF} = 0$	$v_{HF} = 1$	$v_{HF} = 0$	$v_{HF} = 1$
	Intermolecular Stretch			
E_e	−473.8288	−540.4420	−476.7455	−544.9095
ω_e	90.9507	97.1494	91.4096	97.8866
$\omega_e x_e$	4.8697	4.9075	4.8963	4.9697
$\omega_e y_e$	0.0433	0.0501	0.0443	0.0537
	Rotational Constants			
E_0	−429.7320	−493.2816		
B	0.1188	0.1207		
D	9.4×10^{-7}	8.5×10^{-7}		

TABLE 7: Red Shift of HF Stretch Frequency, with Respect to Free HF Value of 3961.23 cm^{-1}

ΔE ($v_{HF} = 1 \leftarrow 0$)	red shift (cm^{-1})	^{37}Cl−^{35}Cl isotope shift (cm^{-1})
harmonic calculations MP2/CCSD(T)[7]	93/79	$<10^{-4}$
2D model	39.86	0.019
2+1D model	63.55	0.032
3D calculations	64.96	0.033
experiment[7]	73.69 (68.77)[a]	0.038 (0.035)[a]

[a] Values in parentheses corrected for He matrix shift, see text.

our calculations for both masses of Cl. Our full 3D model gave a ^{37}Cl−^{37}Cl isotope shift of 0.033 cm^{-1}, in good agreement with experiment. As the red shift itself is mainly caused by the increase of D_0 with the excitation of the HF stretch, the origin of this isotope effect on the red shift is mostly the fact that the intermolecular zero-point energy contained in D_0 is lower for ^{37}Cl−HF than for ^{35}Cl−HF.

The experimental spectrum[7] also produced a value for the rotational constant: $B = 0.055$ cm^{-1} for ^{35}Cl−HF in He clusters. Our ground-state calculated value is: $B = 0.119$ cm^{-1}. The factor of 2.16 is a He cluster effect; a factor of 2−3 is commonly observed for this effect.

3.5. Renner—Teller Effects. It was already mentioned above and in ref 8 that linear Cl−HF is a very typical Renner−Teller system[27] of case 1a,[28] because (in the absence of spin−orbit coupling) it has a 2-fold degenerate electronic ground state of Π symmetry and the bending potential is nearly quadratic in the bend angle. To characterize such systems it is customary following Renner[27] to introduce the quantum number K, which corresponds to the sum of the electronic orbital angular momentum Λ and the vibrational angular momentum l of the bending mode of a linear triatomic system. In our treatment, which includes the full range of angles θ, the relevant electronic angular momentum quantum number is μ, with the values $\mu = \pm 1$ in the diabatic states that dominate the ground-state wave function localized near the linear Cl−HF minimum. The vibrational angular momentum l is given by ω_B. Hence, the Renner−Teller quantum number K is given by $K = \mu + \omega_B$, which can also be written as $K = \Omega - \Sigma = \omega_A + \omega_B - \Sigma$, where $\Sigma = \pm{}^1/_2$ is the component of the spin S on the intermolecular z-axis **R**. The quantum number that is commonly denoted by P corresponds to Ω in our case. The ground state with $|\Omega| = {}^3/_2$ corresponds to $|K| = 1$; i.e., in the Renner−Teller notation,[29] it can be written as $^{2S+1}K_{|P|} = {}^2\Pi_{3/2}$. The same term symbol holds for the accompanying intermolecular stretch progression with v_s ranging from 0 to 7. Most interesting are the bend excited states with $v_b = 1$ and vibrational angular momentum $\omega_B = \pm 1$. They give rise to a bend fundamental with $|\Omega| = {}^1/_2$ denoted by $^2\Sigma_{1/2}$ and a bend fundamental with $|\Omega| = {}^5/_2$ denoted by $^2\Delta_{5/2}$. Both these bend modes are indeed observed, see Table 2, with accompanying bend−stretch combination progressions ranging from $v_s = 0$ to 1 for the $^2\Sigma_{1/2}$ levels and from $v_s = 0$ to 4 for the $^2\Delta_{5/2}$ levels. The fundamental bend frequency for the $^2\Sigma_{1/2}$ levels is 429.55−260.94 = 168.62 cm^{-1} and the first excitation frequency of the $^2\Delta_{5/2}$ levels is 428.96−221.70 = 207.26 cm^{-1}. For the levels that correspond to $v_{HF} = 1$, the $^2\Sigma_{1/2}$ bend frequency is 493.10−305.51 = 187.59 cm^{-1} and the $^2\Delta_{5/2}$ bend frequency is 492.50−264.50 = 227.99 cm^{-1}. These numbers are from the 2 + 1D calculations, because the 3D results for $|\Omega| = {}^5/_2$ are not available. The value for the $^2\Sigma_{1/2}$ levels from 3D calculations is not very different, however.

We may compare our set of levels to the energy level diagram of a $^2\Pi$ triatomic linear molecule shown in Herzberg's book,[29] Figure 8 of section I.2. This diagram correlates the energy levels obtained from a full calculation with the levels obtained when either the Renner−Teller interaction or the spin−orbit coupling is set to zero. Herzberg's "full" treatment includes the bending mode only and it defines the Renner−Teller interaction parameter ϵ as the ratio of the harmonic force constants of the coupling or difference potential $V_{1,-1} = [V(A'') - V_1(A')]/2$ at the linear geometry and the diagonal or sum potential $2V_{1,1} = V_1(A') + V(A'')$. The corresponding set of levels from our calculation is listed in Table 2. Note that the bend quantum number v_b in our notation, is denoted as v_2 in Herzberg's figure. In Herzberg's figure the levels of the same $|K|$ with the larger $|P|$ are higher than the levels with smaller $|P|$, whereas in our case the levels with the larger $|P|$ are lower. The reason for this reversed order is that our spin−orbit constant A has a negative value, while Herzberg's is positive. In that sense, the Cl−HF results may be compared with the level pattern of another Renner−Teller system, $He-HF^+$, calculated in our group earlier[30] (see Figures 4 and 5 of that reference). However, the absolute value of 588.1 cm^{-1} of the spin−orbit parameter A is so large that the upper levels of the spin−orbit doublets in Cl−HF (such as the $^2\Pi_{1/2}$ level that is spin−orbit excited from the ground $^2\Pi_{3/2}$ level) are not bound anymore. Otherwise, the levels from our calculations follow the pattern of the levels in Herzberg's picture of a typical Renner−Teller system.

The substantial splitting between the $^2\Sigma_{1/2}$ and $^2\Delta_{5/2}$ levels that correspond to the same $v_b = 1$ bend fundamental is caused by the Renner−Teller interaction (parametrized in Herzberg's treatment by ϵ), which in our case is represented by the off-diagonal diabatic potential $V_{1,-1}$. In the work on $He-HF^+$[30] it was shown, however, that this splitting does not disappear even when the coupling potential $V_{1,-1}$ is switched off. This is a fundamental deviation from Herzberg's model, which was shown in ref 30 to be due to the fact that the bending motion is treated in our work as a hindered rotation rather than a harmonic vibration as in Renner's work.

4. Conclusion

The preceding paper (ref 8) presents the full 3×3 matrix of diabatic potential surfaces that correlate with the ^2P state of the Cl atom. With the use of these potentials and the inclusion of spin−orbit coupling we computed bound energy levels and properties of the Cl(^2P)−HF complex in full three-dimensional (3D) calculations. Dynamical variables are the Jacobi coordinates: the distance R between Cl and the HF center of mass, the HF bond length r, and the angle θ between the Cl−HF axis **R** and the HF axis. We also made 2D calculations in which the HF bond length r was frozen at the vibrationally averaged values r_0 and r_1 and 2 + 1D calculations in which the 3D potentials were averaged over the $v = 0$ and $v = 1$ vibrational wave functions of free HF. Furthermore, we performed 2D calculations for r frozen at the HF equilibrium value r_e and 1D calculations in which both r and the Cl−HF distance R were frozen. Together, these calculations provided a clear picture of the dynamics of the Cl−HF complex.

The complex is found to have the linear hydrogen bonded Cl−HF structure corresponding to the global minimum in both the diagonal diabatic and the adiabatic potential surfaces, with ground-state quantum numbers $J = {}^3/_2$ and $|\Omega| = {}^3/_2$ and correlating with the $^2P_{3/2}$ ground state of the Cl atom. The bend fundamental with $v_b = 1$ and vibrational angular momentum $\omega_B = \pm 1$, interacting with the electronic $^2\Pi$ ground state with $\mu = \pm 1$, produces levels with $|\Omega| = {}^1/_2$ and $|\Omega| = {}^5/_2$ that are split: the Renner−Teller effect. A series of intermolecular (R) stretch modes was identified and fitted to a Dunham expansion, both for the ground state and for the levels with the HF stretch mode excited. From the levels computed for $J = {}^1/_2$ to ${}^7/_2$ we extracted rotational and distortion constants, as well as e−f parity splittings. The Cl−HF bond, with $D_0 = 432.25$ cm^{-1} for $v_{HF} = 0$ and $D_0 = 497.21$ cm^{-1} for $v_{HF} = 1$, is considerably strengthened when the HF stretch is excited. The computed red shift of the HF stretch frequency of 64.96 cm^{-1} and the $^{35}Cl-{}^{37}Cl$ isotope shift of 0.033 cm^{-1} are in good agreement with the values of 68.77 and 0.035 cm^{-1} obtained from the recent experiment of Merritt et al.[7] after correction for the effect of the He nanodroplet matrix in which they were measured.

Acknowledgment. The authors wish to thank Dr. P. E. S. Wormer, Prof. R. E. Miller, and Dr. J. M. Merritt for stimulating discussions.

References and Notes

(1) Takayanagi, T.; Kurosaki, Y. *J. Chem. Phys.* **1998**, *109*, 8929.
(2) Skouteris, D.; Manolopoulos, D. E.; Bian, W.; Werner, H.-J.; Lai, L.-H.; Liu, K. *Science* **1999**, *286*, 1713−1716.
(3) Takayanagi, T.; Wada, A. *Chem. Phys. Lett.* **2001**, *338*, 195.
(4) Lester, M. I.; Pond, B. V.; Marshall, M. D.; Anderson, D. T.; Harding, L. B.; Wagner, A. F. *Faraday Discuss. Chem. Soc.* **2001**, *118*, 373.
(5) Neumark, D. M. *Phys. Chem. Commun.* **2002**, *5*, 76.
(6) Xie, T.; Wang, D.; Bowman, J. M.; Manolopoulos, D. E. *J. Chem. Phys.* **2002**, *116*, 7461.
(7) Merritt, J. M.; Küpper, J.; Miller, R. E. *Phys. Chem. Chem. Phys.* **2005**, *7*, 67−78.
(8) Fishchuk, A. V.; Wormer, P. E. S.; van der Avoird, A. *J. Phys. Chem. A* **2006**, *110*, 5273.
(9) Alexander, M. H. *J. Chem. Phys.* **1993**, *99*, 6014.
(10) Dubernet, M.-L.; Hutson, J. *J. Chem. Phys.* **1994**, *101*, 1939.
(11) Dubernet, M.-L.; Hutson, J. *J. Phys. Chem.* **1994**, *98*, 5844.
(12) Zeimen, W. B.; Kłos, J. A.; Groenenboom, G. C.; van der Avoird, A. *J. Chem. Phys.* **2003**, *118*, 7340−7352.
(13) Zeimen, W. B.; Kłos, J. A.; Groenenboom, G. C.; van der Avoird, A. *J. Phys. Chem. A* **2003**, *107*, 5110−5121.
(14) Zeimen, W. B.; Kłos, J.; Groenenboom, G. C.; van der Avoird, A. *J. Phys. Chem. A* **2004**, *108*, 9319−9322.
(15) Lonardo, G. D.; Douglas, A. E. *Can. J. Phys.* **1973**, *51*, 434.
(16) Rydberg, R. *Z. Phys.* **1931**, *73*, 376.
(17) Rydberg, R. *Z. Phys.* **1933**, *80*, 514.
(18) Klein, O. *Z. Phys.* **1932**, *76*, 226.
(19) Rees, A. L. G. *Proc. Phys. Soc. London* **1947**, *59*, 998.
(20) Ho, T.-S.; Rabitz, H. *J. Chem. Phys.* **1996**, *104*, 2584.
(21) Groenenboom, G. C.; Colbert, D. T. *J. Chem. Phys.* **1993**, *99*, 9681−9696.
(22) Alexander, M. H.; Manolopoulos, D. E.; Werner, H.-J. *J. Chem. Phys.* **2000**, *113*, 11084.
(23) Jeziorska, M.; Jankowski, P.; Szalewicz, K.; Jeziorski, B. *J. Chem. Phys.* **2000**, *113*, 2957.
(24) Lefebvre-Brion, H.; Field, R. W. *Perturbations in the spectra of diatomic molecules*; Academic: New York, 1986.
(25) Nauta, K.; Miller, R. E. *J. Chem. Phys.* **2000**, *113*, 10158−10168.
(26) Nauta, K.; Miller, R. E. *J. Chem. Phys.* **1999**, *111*, 3426−3433.
(27) Renner, R. *Z. Phys.* **1934**, *92*, 172.
(28) Pople, J. A.; Longuet-Higgins, H. C. *Mol. Phys.* **1958**, *1*, 372−383.
(29) Herzberg, G. *Molecular Spectra and Molecular Structure, Vol. 3: Electronic Spectra and Electronic Structure of Polyatomic Molecules*; Van Nostrand: New York, 1950.
(30) Dhont, G.; Zeimen, W. B.; Groenenboom, G. C.; van der Avoird, A. *J. Chem. Phys.* **2004**, *120*, 103−116.